Kinetics and Catalysis, Vol. 45, No. 6, 2004, pp. 879–889. From Kinetika i Kataliz, Vol. 45, No. 6, 2004, pp. 930–941.

PEROXIDES-XI

Reduction Requirements for Ru/(K)Fe_2O_3 Catalytic Activity in Water–Gas Shift Reaction[1]

W. K. Jóźwiak*, T. P. Maniecki*, A. Basińska, J. Góralski*, and R. Fiedorow****

** Institute of General and Ecological Chemistry, Technical University of Lodz, 90-924 Lodz, Zwirki 36, Poland*
e-mail: wjozwiak@ck-sg.p.lodz.pl.
*** Faculty of Chemistry, Adam Mickiewicz University, 60-780 Poznan, Poland*

Received November 10, 2002

Abstract—This paper is focused upon the influence of potassium on the reduction behavior and catalytic properties of Fe_2O_3, Ru/Fe_2O_3 and Ru/(K)Fe_2O_3 catalysts for the water gas shift (WGS) reaction. The effect of promotion by potassium is attributed to stabilization of a highly dispersed ruthenium phase on the iron oxide surface. The hydrogen reduction behavior of Fe_2O_3 catalysts is strongly influenced by time-pressure dependent processes and comprises two or three heavily overlapped TPR peaks which can be ascribed to the following stages of the iron(III) oxide reduction $3Fe_2O_3 \longrightarrow 2Fe_3O_4 \longrightarrow 6FeO \longrightarrow 6Fe$. The appearance of FeO as an intermediate phase was confirmed by XRD. The presence of ruthenium(IV) oxide substantially changes the kinetics of the reduction process. In the case of potassium-doped catalysts, the reduction of Fe_2O_3 is substantially different and is assigned to the reduction phase of $KFeO_2$. Both ruthenium and potassium have a promoting effect on the catalytic activity for the WGS reaction.

1. INTRODUCTION

The water gas shift (WGS) reaction

$$CO + H_2O \longrightarrow CO_2 + H_2,\ \Delta H = -41.1\ \text{kJ/mol}$$

can be catalyzed by many metals and metal oxides [1]. This process plays an important role in industry and usually is performed in conjunction with production of hydrogen by steam reforming of hydrocarbons [2]. Catalysts based on iron oxides are used in the WGS reaction which proceeds in the temperature range of 400–500°C [1]. The catalysts containing a supported metallic phase (Ru) and doped with alkali metals (Na, K) were also investigated in the WGS process [3]. Despite extensive research efforts, the mechanism of the water gas shift reaction on the iron oxide surface and the exact nature of active sites for WGS reaction are relatively poorly understood [4, 5].

This paper is focused upon the influence of potassium on the reduction behavior and catalytic properties of Fe_2O_3, Ru/Fe_2O_3, and Ru/(K)Fe_2O_3 catalysts for the water gas shift reaction.

2. EXPERIMENTAL

Iron(III) oxide, used as a support for Ru/Fe_2O_3 and Ru/(K)Fe_2O_3 catalysts, was prepared by calcination of iron oxide-hydroxide for 3 h at 600°C in air [5, 6]. The ruthenium catalysts (0.5, 1, and 5% Ru) were obtained by incipient wetness impregnation using $RuCl_3$ aqueous solution, followed by drying at 105°C and 3 h oxidation in air at 350°C. Potassium-doped catalysts contained 3.6% K.

The catalysts were characterized by H_2 chemisorption, TPR_{H2}, TPR_{CO}, TPD, low-temperature N_2 adsorption, TG-DTA-MS, FTIR and XRD techniques.

Thermogravimetric measurements (TG-DTA-MS) were carried out in different atmospheres (H_2, 2% H_2–98% Ar, CO, 5% CO – 95% He, 5% H_2O–95% Ar). The linear heating rates (1 and 10 K/min) were used in the temperature range 20–1000°C. Sample mass was about 20 mg.

Surface area and pore distribution of catalyst samples were determined by Sorptomatic 1900 (Carlo Erba) using low-temperature nitrogen adsorption.

Temperature programmed reduction (TPR) measurements were carried out on an AMI–1 Altamira instrument. Prior to the TPR measurements, catalyst samples (0.2 g) were calcined for 1 h at 350°C in 10% O_2–90% Ar gas stream. The oxidized samples were reduced in 10% H_2–90% Ar gas mixture (flow rate: 50 cm^3/min); heating rates were 1 and 10 K/min. In the case of the latter heating rate, isothermal conditions were maintained for 0.5 h after reaching 900°C.

TPD studies were conducted according to the following procedure: catalysts were activated for 4 h in the stream of CO/H_2O = 1 : 25 at 350°C, cooled down in the above mixture to 100°C, and then desorption was carried out in a stream of argon at a linear temperature increase of 10 K/min up to 950°C.

[1] This article was submitted by the authors in English.

Table 1. Surface areas of Ru/Fe_2O_3 and $Ru/(K)Fe_2O_3$ catalysts Fe_2O_3

Catalyst	Surface area, m^2/g	Calcination temperature, °C
Fe_2O_3	13	600
$(K)/Fe_2O_3$	21	″
0.5% Ru/Fe_2O_3	7	350
0.5% $Ru/(K)Fe_2O_3$	9	″
5.0% Ru/Fe_2O_3	9	″
5.0% $Ru/(K)Fe_2O_3$	13	″

X-ray diffraction (XRD) measurements were performed with a polycrystalline D 5000 Siemens X-ray diffractometer. It operated with a scanning speed of 0.03° step per 5 s. Diffraction patterns were recorded in the range of $2\theta = 20°–80°$ using nickel–filtered CuK_α radiation.

Hydrogen chemisorption measurements were carried out on an ASAP 2010C instrument made by Micromeritics. Sample weight was about 0.5 g. The following procedure was applied: preliminary evacuation and heating at 200°C (1 h), the flow of hydrogen at the same temperature (1 h), evacuation at 200°C (2 h), cooling down to 100°C, leak test and finally the measurement of the hydrogen chemisorption isotherm at 100°C.

Measurements of catalytic activity for the WGS reaction were carried out under atmospheric pressure at 300 or 350°C with a reactant mixture flow rate of 60 cm^3/min and a molar ratio of $H_2O/CO = 2.5$. GC analysis of the reactant mixture was performed after 3 h standardization of the catalyst sample (0.2 g) in WGS conditions.

The catalytic activity was characterized by the conversion of CO (mol %).

3. RESULTS AND DISCUSSION

3.1. Surface Area and Pore Size Distribution

Results of surface area measurements of Fe_2O_3, $(K)Fe_2O_3$, Ru/Fe_2O_3 and $Ru/(K)Fe_2O_3$ catalysts after their calcination in oxygen (4 h) at 600°C (support) and 350°C (support + active phase) are presented in Table 1. Depending on the kind of catalyst, specific surface area ranged from 7–21 m^2/g. The potassium-doped Fe_2O_3 catalyst has considerably higher surface area (by about 60%) than that of undoped Fe_2O_3, whereas surface areas of ruthenium-containing catalysts are lower. Pore size distributions for these catalysts are presented in Figs. 1a and 1b for Ru/Fe_2O_3 and $Ru/(K)Fe_2O_3$ catalysts, respectively. The bimodal character of pore size distribution for Fe_2O_3 undergoes considerable modification as a result of ruthenium and potassium presence on the iron oxide surface. At a ruthenium content of 0.5% a considerable increase in dominant pore radius from 100 to 500 Å is observed. An increase in ruthenium loading to 5% results in a rise in the dominant radius to 200 Å (Fig. 1a). Quite a different textural pattern is shown by the potassium-doped Fe_2O_3 (Fig. 1b) catalyst which is characterized by the presence of micropores (dominant radius of about 16 Å). The introduction of ruthenium to the $(K)Fe_2O_3$ system results in a behavior analogous to that observed for potassium-free catalysts (compare Figs. 1a and 1b).

3.2. Phase Composition

The influence of calcination in oxygen (4 h) at 600 and 900°C on the XRD patterns of Fe_2O_3 and potassium-promoted (K/Fe_2O_3) catalysts is presented in Fig. 2. The effect of the WGS reaction (350°C, 4 h) on phase compositions of the catalysts is shown as well. The phase composition of Fe_2O_3 does not change after oxygen treatment at 600 and 900°C (compare curves (*1*) and (*2*)), whereas a new phase, $KFeO_2$, is formed in the potassium-doped catalyst during its calcination in oxygen. This potassium-iron oxide phase is dominant, especially after oxidation at 900°C (see curves (*3*) and (*4*)). The complete reduction of Fe_2O_3 to Fe_3O_4 has occurred after catalyst treatment in WGS reaction conditions (see curves (*5*) and (*6*)). The identification of ruthenium oxide phase (RuO_2) by means of XRD was not possible both for potassium-free and potassium-doped 5% Ru/Fe_2O_3 catalysts. The major phase, Fe_3O_4, which is present during the WGS reaction, is accompanied by minor FeOOH and FeC phases (in Fig. 2 see curves (*5*) and (*6*)).

The influence of various reduction conditions on the XRD patterns recorded for iron(III) oxide is shown in Fig. 3. Results for the Fe_2O_3 sample subjected to a preliminary oxidation (4 h in O_2 at 600°C) are presented in curve *1*. The subsequent reduction of this sample (4 h in H_2 at 200°C) results in a coexistence of two phases, Fe_2O_3 and Fe_3O_4, which is illustrated by curve *2*. The same pattern was obtained for iron oxide after a TPR_{H2} run (10% H_2 – 90% Ar, 1 K/min) interrupted at 360°C (curve *3*). The analogous shape of the TPR pattern up to 500°C confirms the disappearance of the Fe_2O_3 phase and the coexistence of Fe_3O_4 and FeO phases (see curve *4*). Reduction in pure hydrogen (4 h at 400°C) or carbon monoxide (4 h at 500°C) results in the appearance of only a metallic iron phase (curves *5* and *6*). In the latter case, the iron metal phase is accompanied by the presence of carbon deposits formed as a result of a carbon monoxide disproportionation reaction. The formation of large amounts of carbon was observed on the

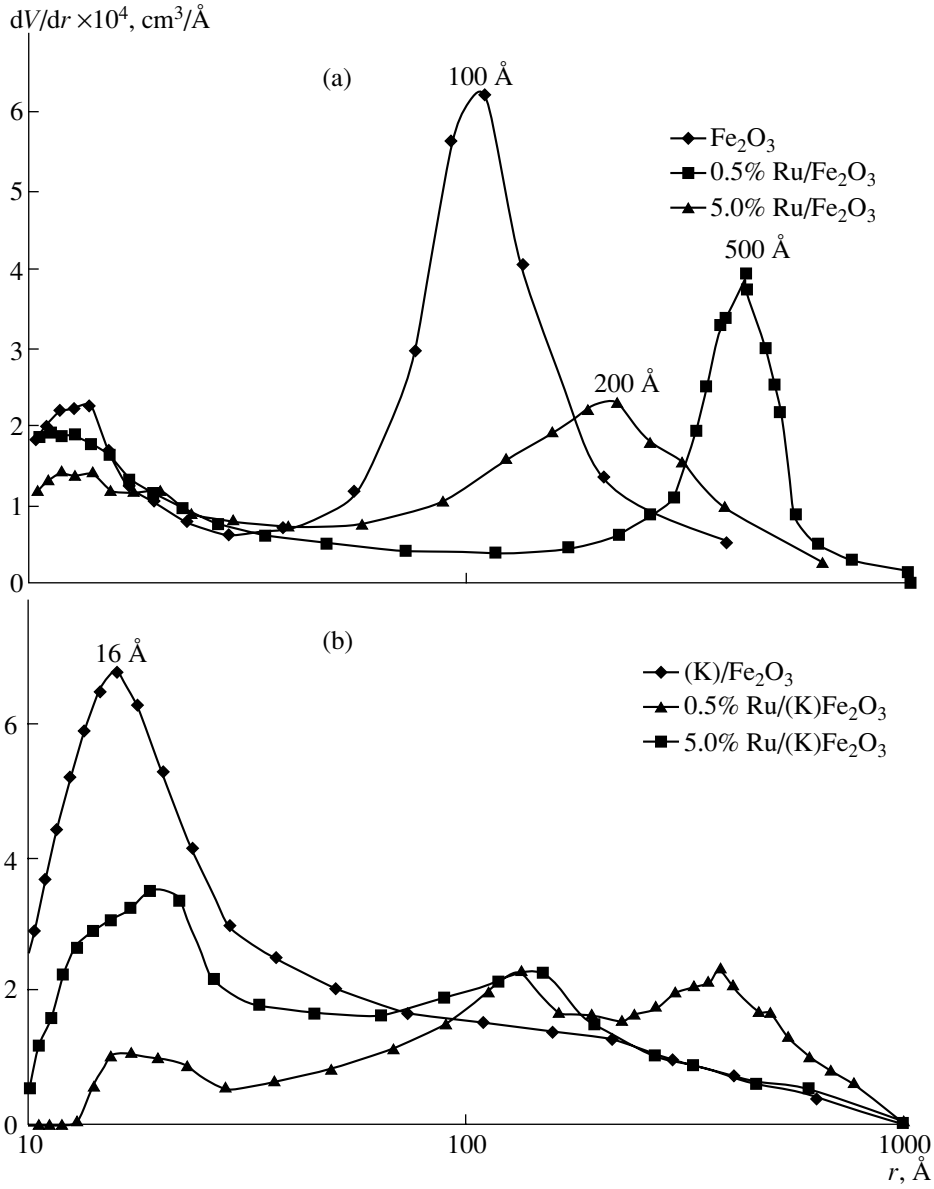

Fig. 1. The influence of ruthenium loading on pore size distribution in Ru/Fe_2O_3 (a) and Ru/(K)Fe_2O_3 (b) catalysts.

hematite layer during calcination in CO as well as during the thermogravimetric analysis of hematite in a carbon monoxide atmosphere (see further on).

3.3. Ruthenium Dispersion

Hydrogen chemisorption on ruthenium catalysts is an activated process which is very slow at room temperature. Therefore, the use of hydrogen uptakes at 100°C was suggested for the determination of ruthenium surface area [7]. For this reason we performed hydrogen adsorption measurements at the above temperature. Although some reduction of iron(III) oxide was expected to occur at 200°C (see curve *2* in Fig. 3), we have chosen the latter temperature for hydrogen pretreatment (prior to adsorption measurements) in order to assure complete reduction of RuO_2 to Ru.

The results of hydrogen chemisorption measurements are given in Table 2. Ruthenium dispersion ranges from about 11 to 90% and higher values were obtained for lower ruthenium loadings. Potassium-promoted ruthenium catalysts show a much higher dispersion of ruthenium than potassium-free catalysts of the same Ru loading. In order to determine the effect of treatment with hydrogen (preceding chemisorption measurements) on the surface area of iron oxide-supported catalysts, the latter was measured both before and after chemisorption experiments. Results of these

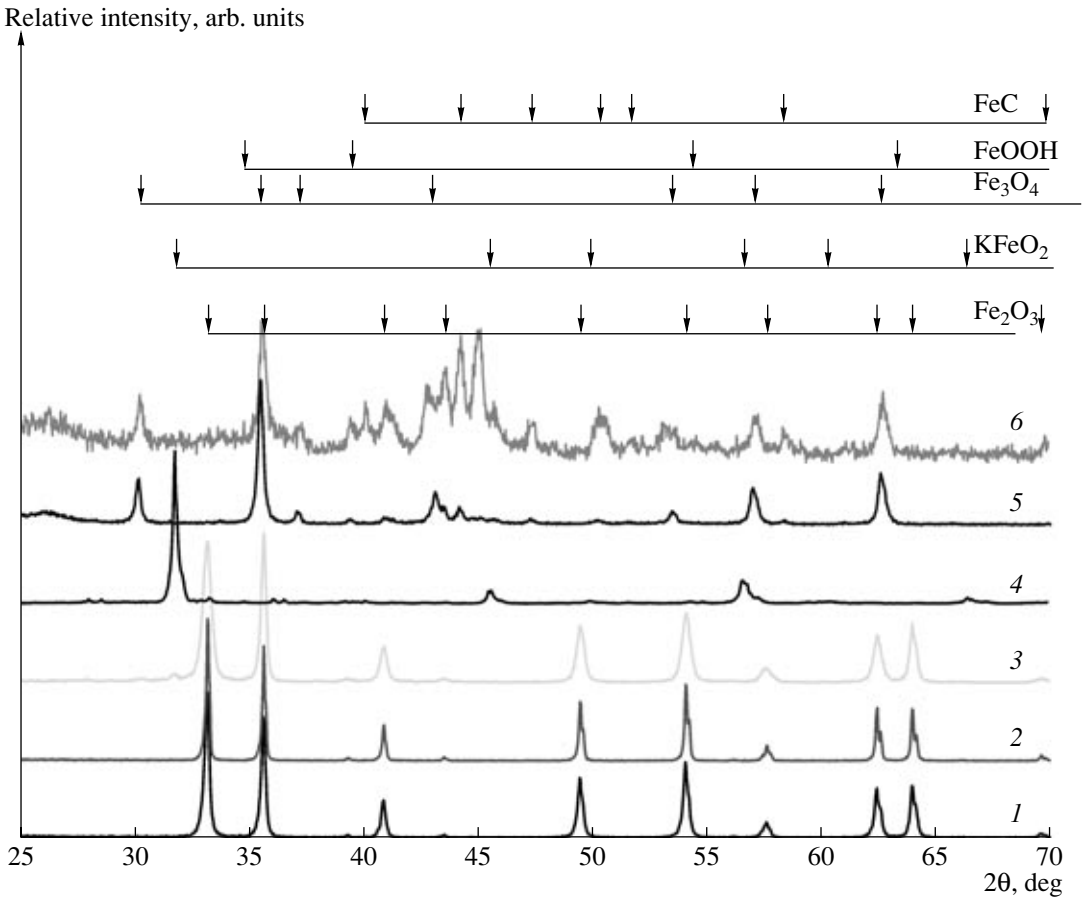

Fig. 2. XRD patterns of Fe_2O_3 pretreated with O_2 and exposed to WGSR for 4 h: (*1*) Fe_2O_3, 600°C, O_2; (*2*) Fe_2O_3, 900°C, O_2; (*3*) (K)Fe_2O_3, 600°C, O_2; (*4*) (K)Fe_2O_3, 900°C, O_2; (*5*) Fe_2O_3, 350°C, WGSR; (*6*) (K)Fe_2O_3, 350°C, WGSR.

measurements, which are presented in Table 3, point to about 20% decrease in surface area after such a treatment. This effect can be assigned to partial reduction of hematite at 200°C taking place during hydrogen pretreatment (see also Fig. 3 curve *2*).

3.4. Catalyst Reduction

Reduction with H_2. The susceptibility of iron(III) oxide to reduction with hydrogen strongly depends on the heating rate and the hydrogen partial pressure in the H_2–Ar stream [8]. TG curves (Fig. 4) show that reduc-

Table 2. Dispersion and surface area of ruthenium as determined by hydrogen adsorption at 100°C

Catalyst	Metal dispersion, %	Metal surface		Adsorbed volume, cm^3/g (STP)
		m^2/g Ru	m^2/g sample	
0.5% Ru/Fe_2O_3	60.0	292.3	1.5	0.333
1.0% Ru/Fe_2O_3	42.1	208.2	2.1	0.474
5.0% Ru/Fe_2O_3	11.6	56.7	2.8	0.645
0.5% Ru/(K)Fe_2O_3	89.3	435.0	2.2	0.495
1.0% Ru/(K)Fe_2O_3	58.3	285.0	2.8	0.647
5.0% Ru/(K)Fe_2O_3	35.4	172.0	8.6	1.962

* Determined from the adsorption of H_2 at 100°C.

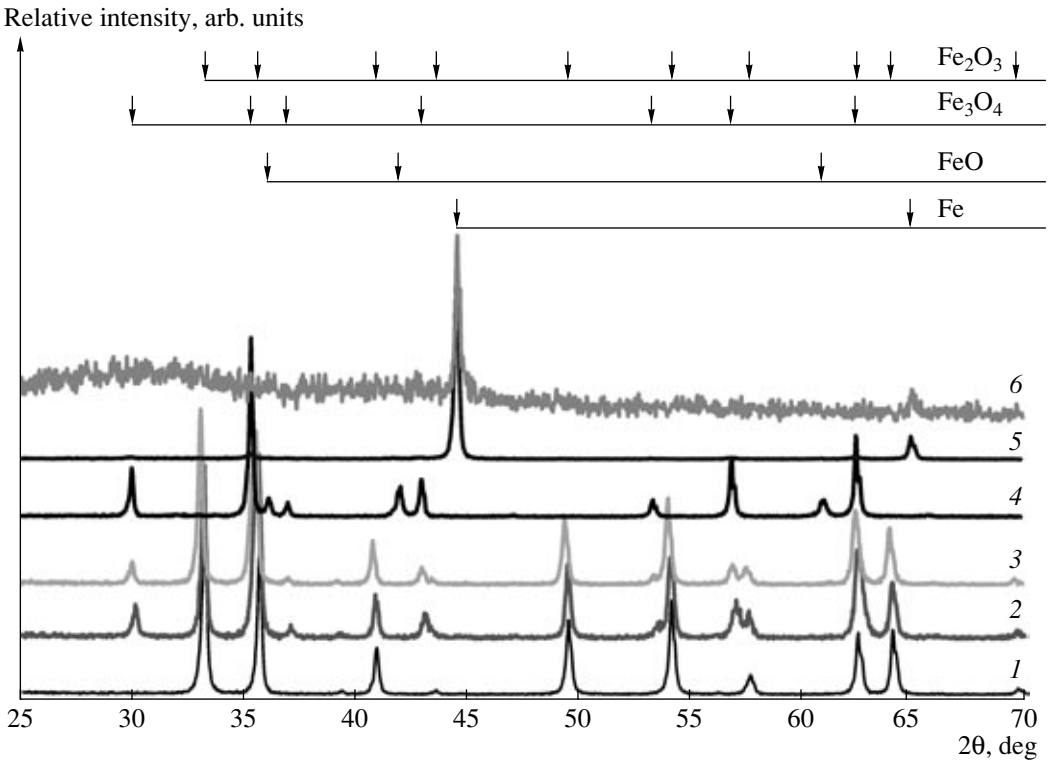

Fig. 3. Reducibility of Fe_2O_3 under various treatment conditions characterized by XRD patterns: (*1*) calcination in O_2 at 600°C for 4 h (original sample), (*2*) original sample reduced at 200°C for 4 h, (*3*) TPR up to 360°C in a 10% H_2–Ar mixture (1 K/min), (*4*) TPR up to 500°C in a 10% H_2–Ar mixture (1 K/min), (*5*) reduction at 400°C in H_2 for 4 h, and (*6*) reduction at 500°C in CO for 4 h.

tion of Fe_2O_3 to Fe metal begins at about 200°C and can be completed at about 390 and 470°C (at heating rates of 1 and 10°C per minute, respectively) in pure H_2 or at 1250°C in a 2% H_2–98% Ar mixture [9–11].

TPR_{H2} profiles for iron oxide-based catalysts, obtained in a 10% H_2–90% Ar mixture, are presented in Figs. 5 and 6 with heating rates of 1 and 10 K/min, respectively. The reduction begins at about 200°C (see Fig. 5) and results in the appearance of two overlapped TPR_{H2} peaks which can be attributed to the following stages of the iron(III) oxide reduction $3Fe_2O_3 \longrightarrow 2\,Fe_3O_4 \longrightarrow 6Fe$ [12]. The presence of ruthenium (from RuO_2) substantially changes the character of the reduction process and three distinct stages are noticeable [13]. The first stage can be assigned to reduction of ruthenium(IV) oxide ($RuO_2 + 2H_2 \longrightarrow Ru + 2H_2O$), the second one to reduction of Fe_2O_3 to Fe_3O_4, and the third stage, at which the reduction reaches 100%, to a gradual transformation of $Fe_3O_4 \longrightarrow FeO \longrightarrow Fe$ which manifests itself as an unresolved peak. The overall process appeared to be limited by a time/temperature–pressure dependent diffusion process and strongly depends on heating rate (compare Figs. 5 and 6). In such conditions, the reduction of $Fe_3O_4 \longrightarrow Fe$ in 10% H_2–90% Ar can be accomplished at 620–1250°C. In pure H_2, the reduction of $3Fe_2O_3 \longrightarrow 2\,Fe_3O_4 \longrightarrow 6Fe$ proceeds in the temperature range of 200–400°C (see Fig. 4). There is no uniform view concerning the mechanism of Fe_2O_3 reduction. According to some literature sources [12], the only intermediate is magnetite, whereas others [14] postulate both magnetite (Fe_3O_4) and wustite (FeO). Our experimental data (from TPR and XRD measurements) prove the existence of a FeO phase as an intermediate in the course of Fe_2O_3 reduc-

Table 3. BET surface area of catalysts before and after hydrogen adsorption measurement

Catalyst	Surface area before chemisorption, m^2/g	Surface area after chemisorption, m^2/g
0.5% Ru/Fe_2O_3	7	6
1.0% Ru/Fe_2O_3	–	–
5.0% Ru/Fe_2O_3	9	6
0.5% Ru/(K)Fe_2O_3	9	7
1.0% Ru/(K)Fe_2O_3	–	–
5.0% Ru/(K)Fe_2O_3	13	12

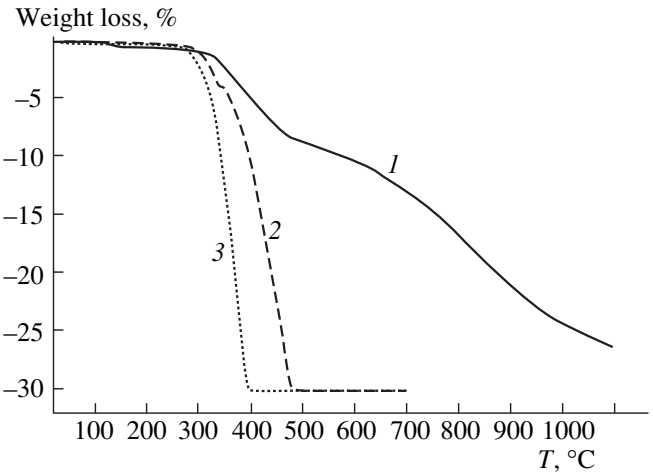

Fig. 4. TG curves for Fe_2O_3 in H_2 stream at different heating rates and H_2 concentrations: (*1*) 2% H_2–98% Ar, 10 K/min; (*2*) 100% H_2, 10 K/min; (*3*) 100% H_2, 1 K/min.

tion regardless of diffusion or kinetic limitations. As can be seen from Figs. 5 and 6, the first step of Fe_2O_3 reduction, i.e., Fe_3O_4 formation, is much easier due to hydrogen spillover from ruthenium on iron(III) oxide (see Fig. 6a). The opposite effect, retardation of magnetite formation caused by potassium, may be attributed to the $KFeO_2$ phase which is considerably more resistant to hydrogen reduction (see Figs. 5 and 6b). Reduction of RuO_2 does not appear as a distinct step of Ru/(K)Fe_2O_3 reduction (see Fig. 6b). In all cases, the overall extent of reduction of Fe_2O_3 to Fe, calculated on the basis of surface areas under TPR curves, was 100%.

Reduction with CO. The susceptibility of iron(III) oxide to reduction with carbon monoxide strongly depends on the heating rate and the carbon monoxide partial pressure in a CO–Ar stream. The relevant TG curves are shown in Fig. 7. The reduction of Fe_2O_3 to metallic Fe begins at about 20°C and can be accomplished in the temperature range of 400–1200°C depending on CO partial pressure and heating rate. The reduction of Fe_2O_3 to iron metal is accompanied by carbon formation in the reaction of carbon monoxide disproportionation: $2CO \longrightarrow C + CO_2$ (compare Fig. 3).

TPR_{CO} measurements were carried out in a gas mixture consisting of 5% CO–95% He which contained trace amounts of O_2 and H_2O of about 300 and 10 ppm, respectively. Thus simultaneous determination of catalyst reduction effects during the reactions of CO oxidation with O_2 and water (WGS) could be followed as a function of increasing temperature. The temperature-controlled sequence of events can be inferred from TPR_{CO} concentration profiles of O_2, H_2, CO_2, and CO recorded for 5% Ru/Fe_2O_3 catalyst and illustrated in Fig. 8a. Starting from the temperature of about 100°C, CO and O_2 are consumed while CO_2 is evolved, which indicates the occurrence of the reaction $CO + 1/2\ O_2 \longrightarrow CO_2$ [9]. In the range 210–245°C, sharp peaks related to CO consumption and CO_2 release are interpreted as reduction of a ruthenium(IV) oxide phase ($RuO_2 + 2CO \longrightarrow Ru + 2CO_2$). From about 230°C, the evolution of hydrogen is observed, resulting from the WGS reaction that proceeds on the ruthenium surface. The maximum concentration of hydrogen occurs at 245°C and at the same temperature the concentration of CO reaches, in practice, its initial level. Most likely, it corresponds to the completion of ruthenium oxide(IV) reduction to metallic ruthenium. Above 245°C, a rapid decrease in the concentration of hydrogen and carbon monoxide is observed, which points to the beginning of hematite reduction to magnetite, reflected by consumption of both CO and H_2 (the latter originates from the WGS reaction). When the above reduction is completed, the concentration of hydrogen in the system again increases and reaches its maximum at 310°C. At higher temperatures, the H_2 concentration decreases once more as it is consumed for further catalyst reduction, and due to the thermodynamic limitations of the WGS reaction, simultaneous desorption of CO and CO_2 is observed at about 500°C. These desorption effects can serve as an indication of catalytic activity for the WGS reaction. Within the temperature range of 320–440°C, the concentration of hydrogen monotonously decreases, in the range of 440–500°C a slight increase in H_2 concentration is observed as a result of the WGS reaction, and in the range of 500–900°C the concentration of H_2 stabilizes at a constant level. The simultaneous desorption of CO and CO_2 is related to the decomposition of a formate-like surface species, according to the equations: $HCOOH \longrightarrow CO_2 + H_2$ and $HCOOH \longrightarrow CO + H_2O$. The evolution of hydrogen was detected during TPD experiments in an Ar stream after the WGS reaction at 350°C. The absence of water evolution can be explained by the subsequent step of iron(II) oxidation: $Fe^{2+} + H_2O \longrightarrow Fe^{3+}–O^- + H_2$.

The analogous TPR_{CO} experiment was performed for the potassium-doped catalyst 5% Ru/(K)Fe_2O_3 (Fig. 8b) in which hydrogen evolution begins at about 280°C due to the WGS reaction that proceeds on the surface of metallic ruthenium. Above 360°C, the hydrogen concentration decreases as a result of its consumption for the reduction of hematite and potassium ferrate(III) ($KFeO_2$), and the decrease is continued up to about 580°C because of the reaction between hydrogen and the evolving oxygen. The latter could originate from peroxide ions O_2^{2-} present in the $KFeO_2$ phase in the potassium-doped catalyst.

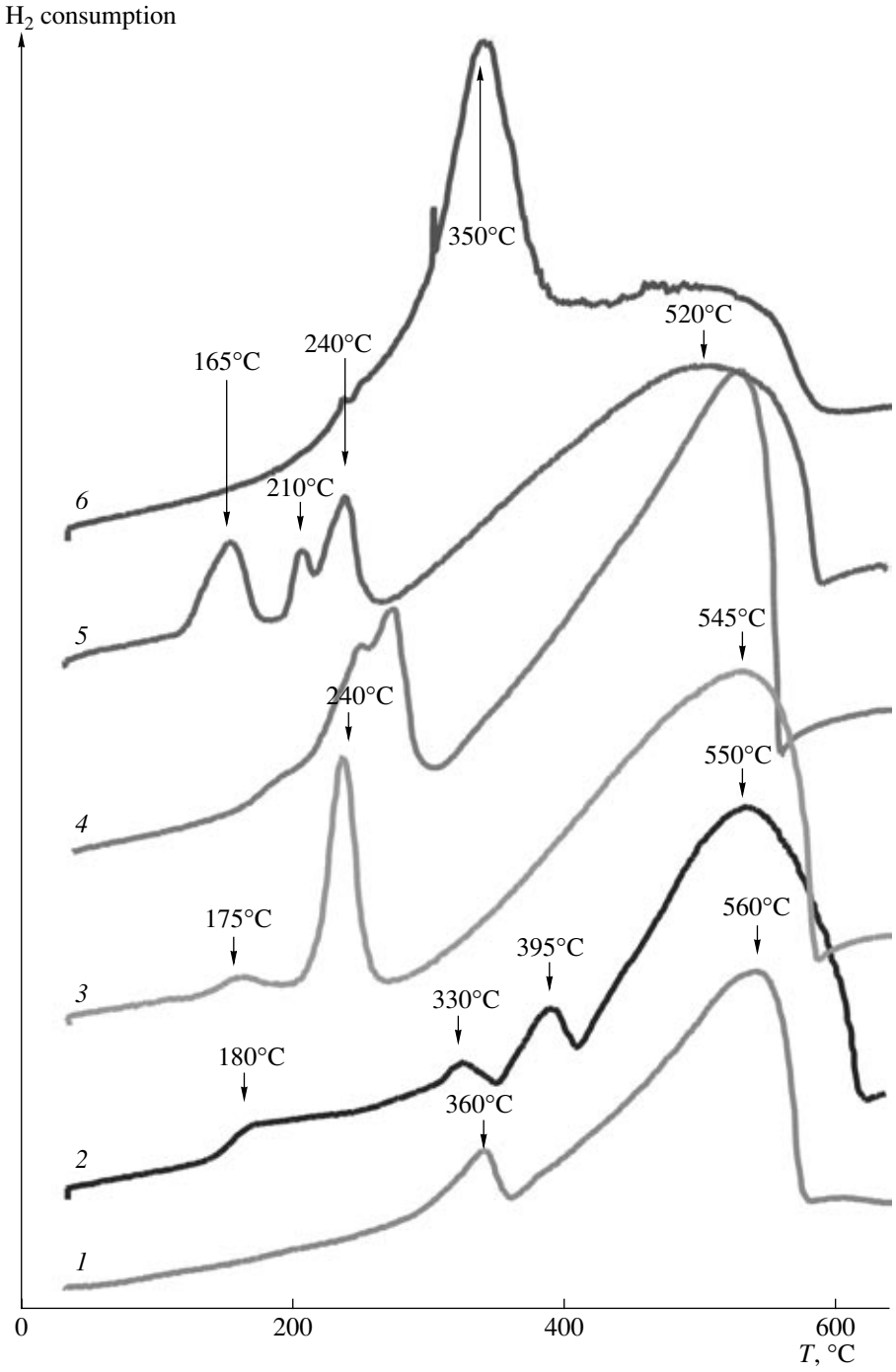

Fig. 5. TPR_{H2} profiles for Fe_2O_3, (K)Fe_2O_3, Ru/Fe_2O_3, and Ru/(K)Fe_2O_3 recorded at a heating rate of 1 K/min: (*1*) Fe_2O_3, (*2*) (K)Fe_2O_3, (*3*) 1% Ru/Fe_2O_3, (*4*) 1% Ru/(K)Fe_2O_3, (*5*) 5% Ru/Fe_2O_3, and (*6*) 5% Ru/(K)Fe_2O_3.

3.5. Catalyst oxidation studied by TPO_{H_2O}

Water, which is the product of the reduction of Fe_2O_3 catalyst with H_2, plays both an important role as a reactant in the WGS reaction and can serve as an oxidant of the iron metallic phase. Fe_2O_3 and Ru/Fe_2O_3 catalysts, previously subjected to complete reduction, were oxidized in a 5% H_2O–95% Ar stream. The results of TG measurements performed in the above gas mixture are presented in Fig. 9. Reoxidation of iron, $Fe + H_2O \longrightarrow Fe_2O_3 + H_2$, proceeds in the temperature range 25–800°C and is promoted by the ruthenium phase. TG-DTG-DTA results for completely reduced Fe_2O_3 sample are presented in Fig. 10. Four endothermic effects in the DTA curve can be assigned to the strongly overlapping following stages: simultaneous

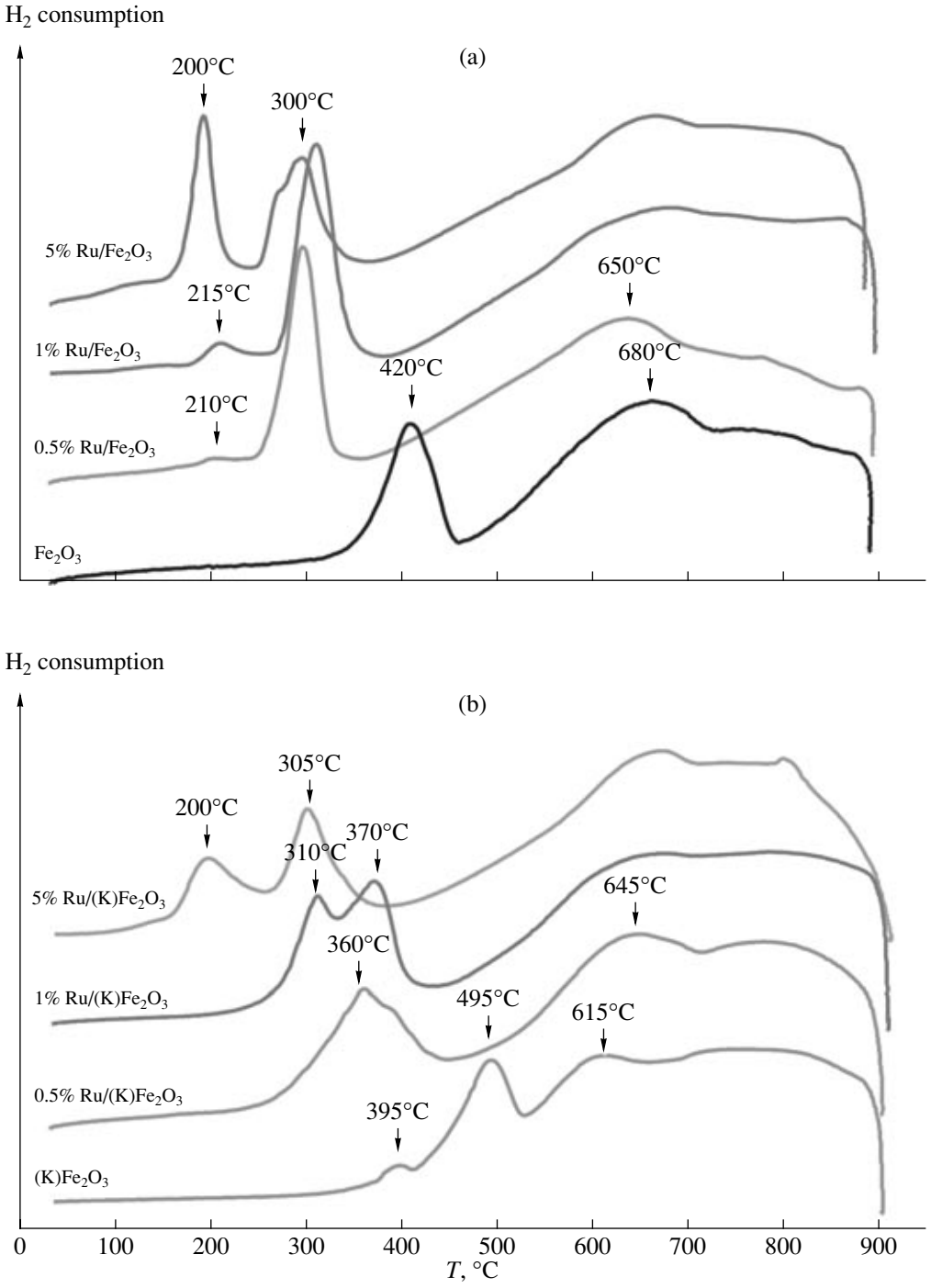

Fig. 6. TPR_{H2} profiles for Fe_2O_3, Ru/Fe_2O_3 (a) and $(K)Fe_2O_3$, $Ru/(K)Fe_2O_3$ (b) recorded at a heating rate of 10 K/min.

formation of an oxy-hydroxy layer on iron and intense dehydration (up to 300°C), wustite formation (300–550°C), magnetite formation (550–620°C) and finally transformation into hematite (up to 800°C). Total increase in sample mass and three positive DTG signals allow us to suggest that the oxidation process proceeds in three stages: $Fe \longrightarrow FeO \longrightarrow Fe_3O_4 \longrightarrow Fe_2O_3$; the sequence is in reverse, compared with that observed during the Fe_2O_3 reduction with H_2.

3.6. Activity for the WGS Reaction

Catalytic activity for the WGS reaction at 300 and 350°C was presented in Table 4. Iron oxide catalysts,

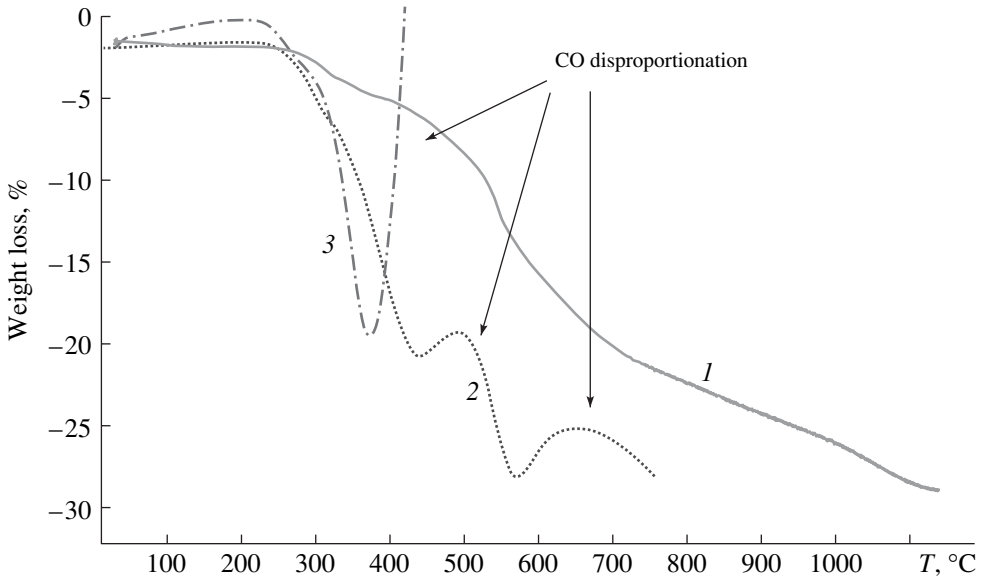

Fig. 7. TG curves for Fe_2O_3 in a CO stream at different heating rates and CO concentrations—the effect of CO disproportionation: (*1*) 5% CO–95% H_2, 10 K/min; (*2*) 5% CO–95% H_2, 1 K/min; and (*3*) 100% CO 1 K/min.

both alone and potassium-doped, were practically inactive for the WGS reaction (carbon monoxide conversion at 350°C was as low as about 6%). The potassium-free 0.5% Ru/Fe_2O_3 catalyst also appeared to be inactive, but when potassium was added, this catalyst of low ruthenium content was characterized by CO conversions of about 21 and 85% at 300 and 350°C, respectively. At higher ruthenium loadings, CO conversions at 350°C on potassium-doped catalysts were clearly above 90%.

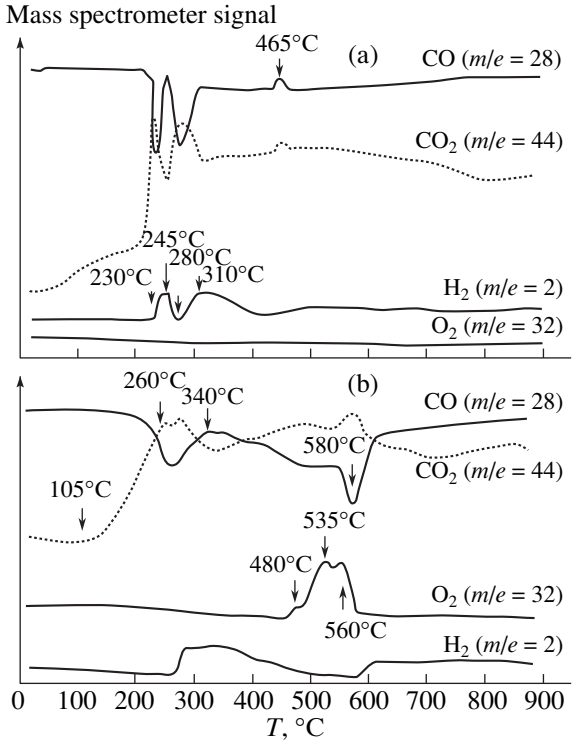

Fig. 8. TPR_{CO} profiles for 5% Ru/Fe_2O_3 (a) and 5% Ru/(K)Fe_2O_3 (b).

3.7. Studies of WGS Active Surface by the TPD Method

Catalytically active surface should enable easy access and removal of compounds involved in the reaction to and from active sites. A useful tool for studying the active surface is temperature programmed desorption, which we have performed according to the procedure described in the experimental section. The desorp-

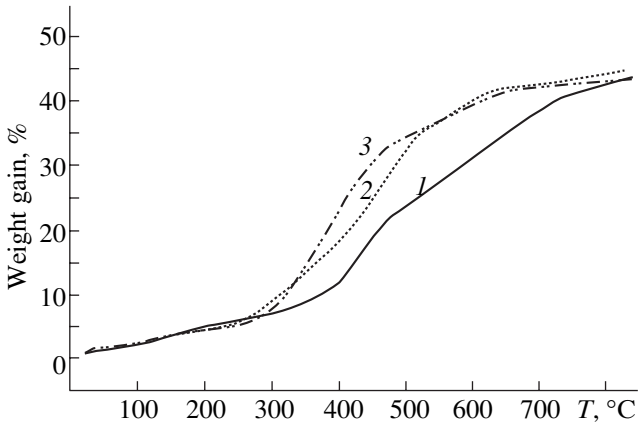

Fig. 9. TG curves recorded for completely prereduced Fe_2O_3 and Ru/Fe_2O_3 catalysts during their treatment with a 5% H_2O–95% Ar mixture: (*1*) Fe, (*2*) 0.5% Ru/Fe, and (*3*) 5% Ru/Fe.

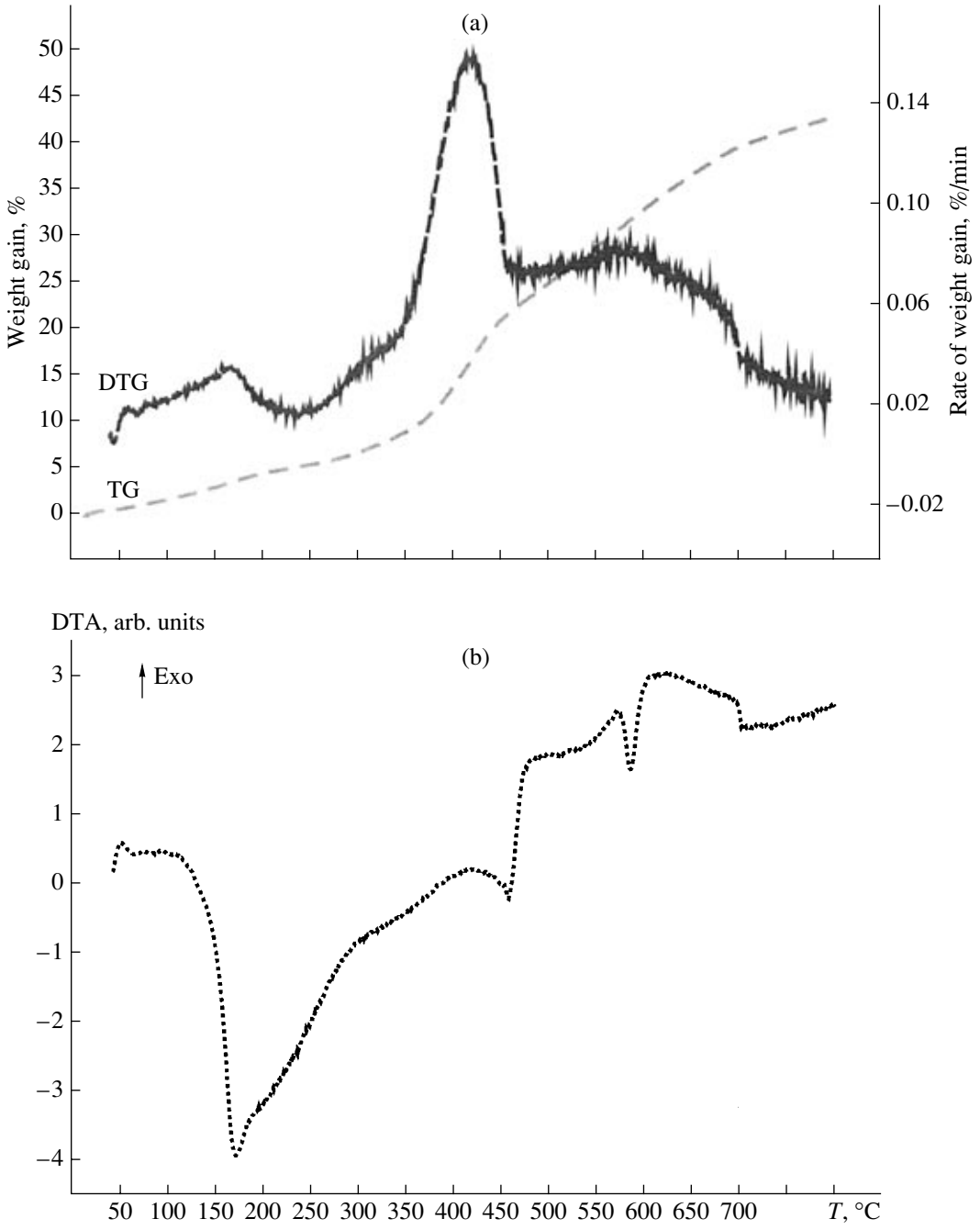

Fig. 10. TG–DTG (a) and DTA (b) study on the completely reduced Fe_2O_3 sample in 5% H_2O–95% Ar.

tion of species present on catalyst surfaces after 4 h on-stream in a WGS reaction at 350°C is shown in Figs. 11a and 11b for the most active potassium-free and potassium-doped 5% Ru/Fe_2O_3 catalysts, respectively (for their catalytic activity—see Table 4). They differ slightly in CO desorption effects, which appear at 400–650°C, and significantly in CO_2 and H_2 desorption effects. The CO/CO_2 molar ratio is close to 1 for the potassium-doped catalyst but much higher ($CO/CO_2 > 5$) for the potassium-free catalyst. Thus, a comparable coverage by CO and CO_2 on the magnetite surface seems to meet the requirement for the best catalyst performance in the WGS reaction. The rate of the WGS reaction is almost independent of H_2 and H_2O concentrations when water is in excess of the stoichiometric amount. Further, more detailed, studies are in progress.

Two kinds of catalytic sites responsible for the WGS reaction are postulated: one is Ru(O) located on the

Table 4. Catalytic activity for WGS reaction

Catalyst	Conversion of CO, % mol*	
	at 350°C	at 300°C
(K)Fe_2O_3 (600°C)	6.2	0.0
(K)Fe_2O_3 (900°C)	0.0	0.0
Fe_2O_3 (600°C)	1.6	0.0
Fe_2O_3 (900°C)	0.0	0.0
0.5% Ru/(K)/Fe_2O_3	84.6	21.2
0.5% Ru/Fe_2O_3	1.1	0.0
1% Ru/(K)/Fe_2O_3	92.2	47.7
1% Ru/Fe_2O_3	90.4	15.1
5% Ru/(K)/Fe_2O_3	94.7	86.1
5% Ru/Fe_2O_3	88.2	49.3

* Measured after catalyst operation for 3.5 h.

ruthenium surface, and the other belongs to the Fe_3O_4 surface. The preliminary condition for high activity is a partial reduction of the catalyst at low temperatures. The ability of the catalyst surface to adsorb carbon dioxide and carbon monoxide can serve as a measure of the concentration of active sites on the iron oxide surface. Lower activity of the magnetite surface results in smaller CO_2 and CO desorption effects and in an increase of the CO/CO_2 ratio.

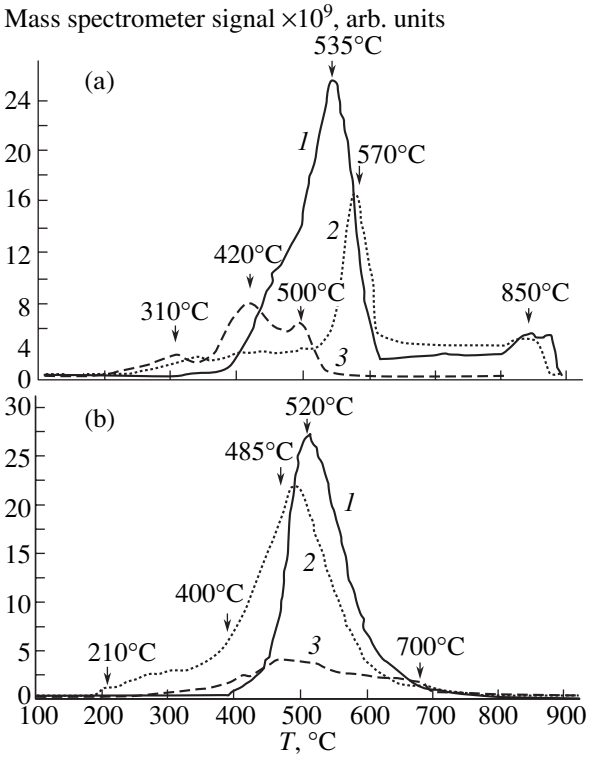

Fig. 11. Temperature programmed desorption from 5% Ru/Fe_2O_3 (a) and 5% Ru/(K)Fe_2O_3 (b) catalysts, performed after WGS reaction (350°C, 4 h): (*1*) CO, *m/e* = 28; (*2*) CO_2, *m/e* = 44; (*3*) H_2, *m/e* = 2.

CONCLUSIONS

The mechanism of hematite reduction by hydrogen presented by the scheme: $3Fe_2O_3 \longrightarrow 2Fe_3O_4 \longrightarrow 6FeO \longrightarrow 6Fe$ involves both magnetite and wustite intermediates, regardless of diffusion and kinetic limitations. Reduction of hematite by carbon monoxide proceeds in a similar way. The mechanism of metallic iron oxidation by water or oxygen is postulated to occur in the reverse direction.

The highest activity for the WGS reaction on a magnetite surface is assured by comparable CO and CO_2 coverages, which are characteristic of potassium-doped Ru/Fe_2O_3 catalysts.

Both ruthenium and potassium strongly influence the promotional effects in reduction and in WGS activity of iron(III) oxide catalysts.

Potassium leads to the formation of a $KFeO_2$ phase which stabilizes the ruthenium phase on the magnetite surface.

REFERENCES

1. Grenoble, D.C.E. and Stadt, M.M., *J. Catal.*, 1981, vol. 67, p. 90.
2. Chenier, P.J., *Survey of Industrial Chemistry*, New York, Kluwer/Plenum, 2002, pp. 45–49.
3. Basińska, A. and Domka, F., *Catal. Lett.*, 1997, vol. 43, p. 59.
4. Boreskov, G.K., Youreva, T.M., and Sergeeva, A.S., *Kinetics and Catalysis*, 1970, vol. 6, p. 1476.
5. Fott, P., Vosolsobe, J., and Glaser, V., *Collection Czechoslov. Chem. Commun.*, 1979, vol. 44, p. 652.
6. Schwertmann, U. and Cornell, R.M., *Iron Oxides in the Laboratory*, Weinheim: Wiley-VCH, 2000.
7. Lu, K. and Tatarchuk, B.J., *J. Catal.*, 1987, vol. 106, p. 166; Dalla Beta, R.A., *J. Catal.*, 1974, vol. 34, p. 57; Taylor, K.C., *J. Catal.*, 1975, vol. 38, p. 299.
8. Vimmers, O.J., Arnoldy, P., and Moulijn, J.A., *J. Phys. Chem.*, 1986, vol. 90, p. 1331.
9. Basińska, A., Jóźwiak, W.K., Góralski, J., and Domka, F., *Appl. Catal.* A: 2000, vol. 190, p. 107.
10. Kadkhodayan, A. and Brenner, A., *J. Catal.*, 1989, vol. 117, p. 311.
11. Tiernan, M.J., Barnes, P.A., and Parkes, G.M., *J. Phys. Chem. B*, 2001, vol. 105, p. 220.
12. Basińska, A., Jóźwiak, W.K., Góralski, J., *et al.*, International Congress on Catalysis, Granada, 2000.
13. Rynkowski, J.M., Paryjczak, T., Lewicki, A., *et al.*, *React. Kinet. Catal. Lett.*, 2000, vol. 71, p. 55.
14. Mingting, Xu and Iglesia, E., *J. Phys. Chem. B*, 1998, vol. 102, p. 961.